

Article

Fabrication of an Ultra-Fine Grained Pure Titanium with High Strength and Good Ductility via ECAP plus Cold Rolling

Haoran Wu ¹, Jinghua Jiang ^{1,2,*}, Huan Liu ^{1,3,*} , Jiapeng Sun ¹ , Yanxia Gu ¹, Ren Tang ¹, Xincan Zhao ¹ and Aibin Ma ^{1,2}

¹ College of Mechanics and Materials, Hohai University, Nanjing 211100, China; haoranwuted@163.com (H.W.); sunpengp@hhu.edu.cn (J.S.); guyanxaj@126.com (Y.G.); 18262636237@163.com (R.T.); xincan_zhao@163.com (X.Z.); aibin-ma@hhu.edu.cn (A.M.)

² Suqian Institute, Hohai University, Suqian 223800, China

³ Jiangsu Wujin Stainless Steel Pipe Group Company Limited, Changzhou 213111, China

* Correspondence: jinghua-jiang@hhu.edu.cn (J.J.); liuhuanseu@hhu.edu.cn (H.L.); Tel.: +86-025-8378-7239 (J.J. & H.L.)

Received: 6 November 2017; Accepted: 8 December 2017; Published: 14 December 2017

Abstract: Microstructure evolutions and mechanical properties of a commercially pure titanium (CP-Ti, grade 2) during multi-pass rotary-die equal-channel angular pressing (RD-ECAP) and cold rolling (CR) were systematically investigated in this work, to achieve comprehensive property for faster industrial applications. The obtained results showed that the grain size of CP-Ti decreased from 80 μm of as-received stage to 500 nm and 310 nm after four passes and eight passes of ECAP, respectively. Moreover, abundant dislocations were observed in ECAP samples. After subsequent cold rolling, the grain size of ECAPed CP-Ti was further refined to 120 nm and 90 nm, suggesting a good refining effect by combination of ECAP and CR. XRD (X-ray diffractometer) analysis and TEM (transmission electron microscope) observations indicated that the dislocation density increased remarkably after subsequent CR processing. Room temperature tensile tests showed that CP-Ti after ECAP + CR exhibited the best combination of strength and ductility, with ultimate tensile strength and fracture strain reaching 920 MPa and 20%. The high strength of this deformed CP-Ti originated mainly from refined grains and high density of dislocations, while the good ductility could be attributed to the improved homogeneity of UFG (ultra-fine grained) microstructure. Thus, a high strength and ductility ultra-fine grained CP-Ti was successfully prepared via ECAP plus CR.

Keywords: commercially pure titanium; rotary-die equal-channel angular pressing; cold rolling; ultra-fine grain; tensile property

1. Introduction

Titanium and its alloys have been widely used in many key fields, such as medical apparatus and instruments, ships, ocean industries, and so on. Among them Ti-6Al-4V alloy is the most commonly used due to its excellent mechanical property and corrosion resistance [1]. However, Ti-6Al-4V alloy is much more expensive than commercially pure titanium (CP-Ti), and the toxicity of the elements vanadium, aluminum and their corrosion products need to be concerned when using in biomedical fields [2]. Therefore, there is a strong need to develop a substitution for Ti-6Al-4V alloy. Grade 2 CP-Ti (TA2) with much lower cost, exhibits a similar corrosion resistance as titanium alloy, but with relatively low mechanical properties (especially its poor strength) [3]. Hence lots of efforts still need to be made to improve the strength of CP-Ti.

Grain refinement is an effective way to improve both strength and plasticity of polycrystalline metallic materials, and the improvement of strength follows a well-known Hall-Petch relationship

approximately [4–6]. Therefore, the ultra-fine grained (UFG) metallic materials with an average grain size of 0.1–2 μm usually exhibit higher strength and ductility, compared with the coarse grained (CG) counterparts [7,8]. Severe plastic deformation (SPD), as a common technique to transform CG microstructure to UFG level, has been widely employed in fabricating bulk UFG aluminum and magnesium alloys without residual porosity and impurities [9–12]. In addition, recently various SPD technologies have been used to prepare high strength CP-Ti [13,14]. Terada et al. [13] employed accumulative roll-bonding (ARB) and successfully developed an UFG CP-Ti with grain size of 80–100 nm, which exhibited an ultimate tensile strength of 989 MPa and elongation of 10%. Stolyarov et al. [14] combined ECAP and cold rolling (CR) on CP-Ti, and prepared an UFG pure Ti (grain size lower than 170 nm) with the highest ultimate tensile strength of 1050 MPa, but with a poor elongation of 6%. It can be seen from the above studies that the SPD CP-Ti exhibited relatively high strength, but their elongations were generally lower than 10%.

Among various SPD techniques, equal channel angular pressing (ECAP) is one of the most promising techniques, which could prepare UFG material without changing the original shape of the materials [15–18]. Moreover, ECAP can easily produce large block material and displays great potential in industrial application [17]. Unfortunately, traditional ECAP processes with B_c route need to take the sample out of the die and rotate after each pass [14,19,20]. Furthermore, reheating is also needed before each new pass, which increases the complexity of processing and causes energy consumption, making it inefficient for large-scale industrial application. To solve this problem, Nishida et al. [21] developed a rotary-die ECAP (RD-ECAP), which tactfully avoids the limitation of the taking sample out and re-inserting procedure, consequently reducing the reheating procedure after each pass. As an ECAP process having a very wide application foreground, the ultimate value of grain refinement of RD-ECAP needs more attention. However, so far, little work has been reported on evolutions of microstructures and mechanical properties of CP-Ti during RD-ECAP, and without repeated annealing during each pass with B_c route, the microstructure evolutions and strengthening mechanism in higher passes of ECAP might be different.

Therefore, in this paper we systematically investigated the microstructure evolutions and mechanical properties of CP-Ti during multi-pass successive RD-ECAP processing. In addition, to refine the microstructure and improve its property more effectively, a cold rolling (CR) processing was further employed on the RD-ECAP CP-Ti. By means of this RD-ECAP + CR combined procedures, an UFG (almost nano-grained, grain size of 90 nm) CP-Ti with better comprehensive mechanical property than previous works was successfully developed, and its ultimate tensile strength and elongation reached 912 MPa and 21.3%, respectively. Moreover, we have also discussed the strengthening and toughening mechanism for this high strength and ductility CP-Ti, in order to provide sufficient guidance on preparing high-performance pure Ti by tuning the grain size and sub-microstructure.

2. Materials and Methods

The raw material used is commercially pure titanium (grade 2), and its composition is analyzed and listed in Table 1. The raw material was hot-forged rod with diameters of 200 mm and in annealed condition (TA2, Baoji Feiteng Metal Materials Co., Ltd., Baoji, China). The average grain size of the original material sample was around 80 μm .

The as-received rod was cut into cuboid billets with dimension of 19.5 mm \times 19.5 mm \times 45 mm for RD-ECAP. To remove the contaminations (oil, debris, etc.) on the surface, the samples were mechanical polished and ultrasonic cleaned in an acetone bath before RD-ECAP. Figure 1a shows the diagrammatic drawing of RD-ECAP, and the detailed information was described in reference [22,23]. The die was designed to have two perpendicular channels with equal cross-section. The channel angle is 90° and the curvature angle is zero. The die rests on the die holder, which have a removable bottom plate and a rigidly side plate, so the side plate can give some back pressure to the billet. There are four punches surrounding the cuboid sample, which can be denoted as bottom vertical punch, right horizontal

punch, left horizontal punch and top vertical punch. When we start the ECAP process, the movement of the bottom vertical punch and right horizontal punch are confined by plate, and only left horizontal punch can move. Then the sample is pressed by the plunger and top vertical punch into the left horizontal channel and the first pass is finished. Rotating the die by 90° clockwise makes the die return to the initial state. Using this method, we can continuously make subsequent passes without taking the sample out each pass. All the punches and samples have been lubricated by molybdenum disulphide and graphite. Before the first pass and every four passes of ECAP, the sample was kept in the die and heated at 693 K for 10 min. Then the sample was continuously pressed for 4 and 8 ECAP passes at the processing speed of $0.5 \text{ mm} \cdot \text{s}^{-1}$. The effective strain of per pass in RD-ECAP is about 1.15 [22].

Table 1. Analyzed composition of commercially pure titanium in this paper (wt %).

Element	C	Fe	O	N	H	Ti
Content	0.015	0.059	0.062	0.013	0.002	balance

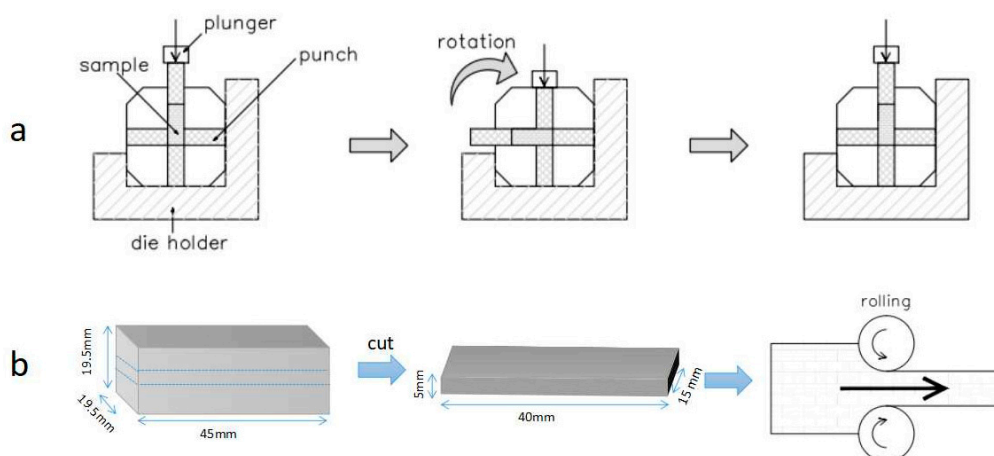


Figure 1. The diagrammatic drawing of (a) RD-ECAP (rotary-die equal-channel angular pressing) and (b) cold rolling.

In order to further refine grains, cold rolling (CR) was employed on ECAP samples. CR samples were cut from the central part of ECAP cuboid with slice thickness of 5 mm (shown in Figure 1b). These slices were also polished to avoid rough surface. Rolling of the slices were carried out on a 300 ton rolling mill at room temperature at a rolling speed of $0.1 \text{ m} \cdot \text{s}^{-1}$ with a total CR strain of 85%. After 8 cycles of rolling, the thickness of slices reached 0.2 mm, and no surface cracking was observed. The accumulative strains for samples after 4 passes ECAP + CR and 8 passes ECAP + CR are about 7.3 and 9.5, respectively.

Microstructure observations of as-received, ECAP and ECAP + CR samples were carried out by an optical microscope (OM, Olympus BHM, Tokyo, Japan), a scanning electron microscope (SEM, S-4800, Hitachi Ltd., Tokyo, Japan), and a transmission electron microscope (TEM, Tecnai G2 20, Field Electron and Ion Company, Hillsboro, OR, USA). Sample for OM observations were mechanically ground, polished, and chemically etched with 3 mL HF, 7 mL HNO₃ and 90 mL distilled water for 15 s. Tensile fracture samples for SEM observations were cleaned by ultrasonic cleaners with absolute ethyl alcohol for 10 min, and then dried by an electric hair dryer. TEM specimens were mechanically thinned to around 65 μm and then twin jet polished in a solution of 6% perchloric acid and 94% ethanol with the operating voltage of 200 KV. Moreover, phase identification was also conducted for all samples by X-ray diffractometer (XRD, Bruker D8 X-ray facility, Karlsruhe, Germany) using CuK α irradiation (45 KV, 30 mA) at a scanning step of 0.5° and exposure time of 1 s from 30° to 80°. Tensile test was conducted by an electronic universal testing machine (TFW-50S, Shanghai Tuofeng

Instrument Technology Co., Ltd., Shanghai, China) at room temperature (298 K) with the displacement rate of $1 \text{ mm} \cdot \text{min}^{-1}$. The tensile samples were machined to be dog bone stick shape with gauge length of 6 mm, gauge width and thickness of 2 mm. For each stage, at least three tensile samples were tested and the final curve which was closest to the average of the tests was selected.

3. Results and Discussions

3.1. Microstructure of As-Received and ECAP CP-Ti (Equal-Channel Angular Pressed Commercially Pure Titanium)

Figure 2 shows the XRD patterns of CP-Ti at all processing stages. For the as-received sample, all diffraction peaks correspond to α -Ti (hexagonal close-packed lattice structure). After multi-pass ECAP and CR processing, the locations of diffraction peaks remain unchanged, although the intensity of some peaks exhibits obvious change. Since there is no other phase detected by XRD for all samples, it can be confirmed that phase transformation was not activated during severe deformation in this work.

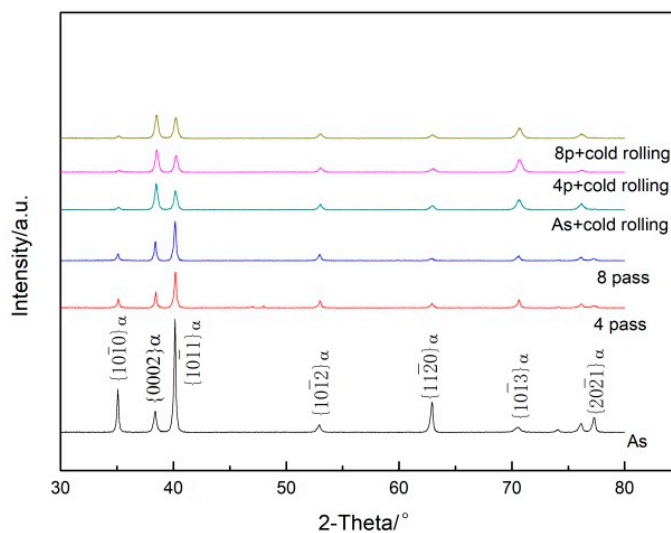


Figure 2. XRD (X-ray diffractometer) patterns of the CP-Ti (Commercially pure Titanium) at different processing stages.

Figure 3a shows the optical micrograph of the as-received CP-Ti. It is apparent that the as-received CP-Ti exhibits equiaxed grains with average grain size of $80 \mu\text{m}$. Moreover, twins are also visible in some grains. Figure 3b,c displays the optical micrograph of ECAP CP-Ti after 4 passes and 8 passes, respectively. The grain size has been refined obviously, and abundant dislocation tangles can be observed. In addition, the twins which existed in as-received CP-Ti is barely observed after ECAP. To further explore the microstructure of ECAP CP-Ti and characterize their grain sizes, TEM observations were performed.

Figure 4a,b shows the TEM micrographs and corresponding SAED (selected area electron diffraction) patterns of ECAP samples after 4 passes and 8 passes, respectively. After 4 passes of RD-ECAP, it can be seen from Figure 4a that the grain size is refined to about 500 nm , and several grains are marked by white arrows in the figure. With increasing the number of ECAP passes to 8, the average grain size is decreased to 310 nm approximately, as is shown by arrows in Figure 4b. It should be noted that the decrease in grain size is significant compared with as-received CP-Ti. Moreover, it can be seen that the diffraction rings were intensive from corresponding SAED patterns, which also indicates that the grain size has been well refined. Moreover, Figure 4c shows that the density of dislocations is very high in 4p-ECAP CP-Ti, and distinct dislocation tangles can be easily observed. However, seen from Figure 4b, dislocation cells and sub-grain boundaries can be easily observed in 8p-ECAP CP-Ti, and the density of dislocations is decreased compared with 4p-ECAP sample.

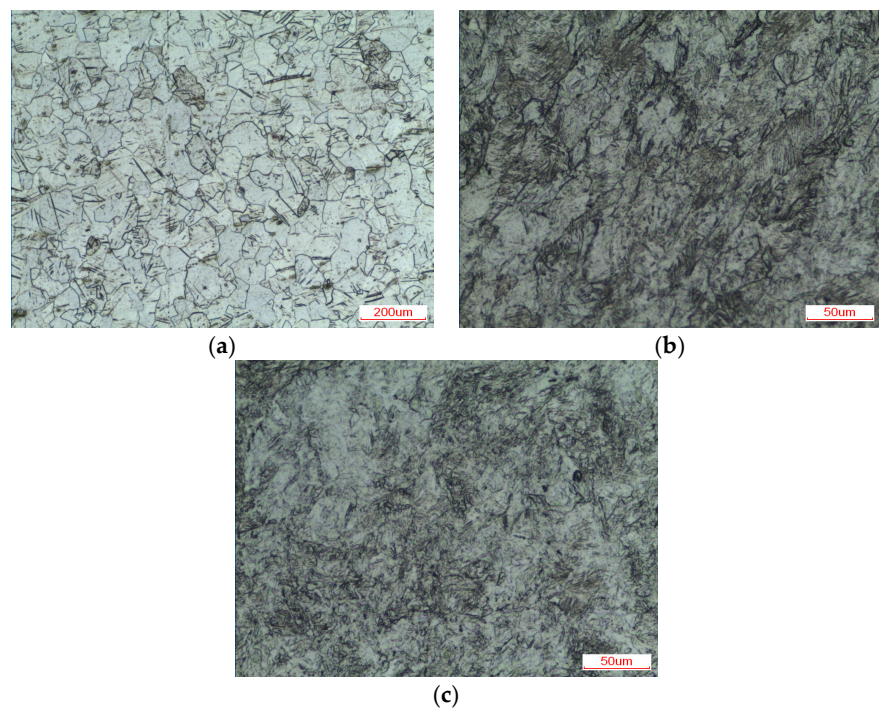


Figure 3. Optical micrographs of CP-Ti at different processing stages: (a) as-received; (b) after 4 passes ECAP; (c) after 8 passes ECAP.

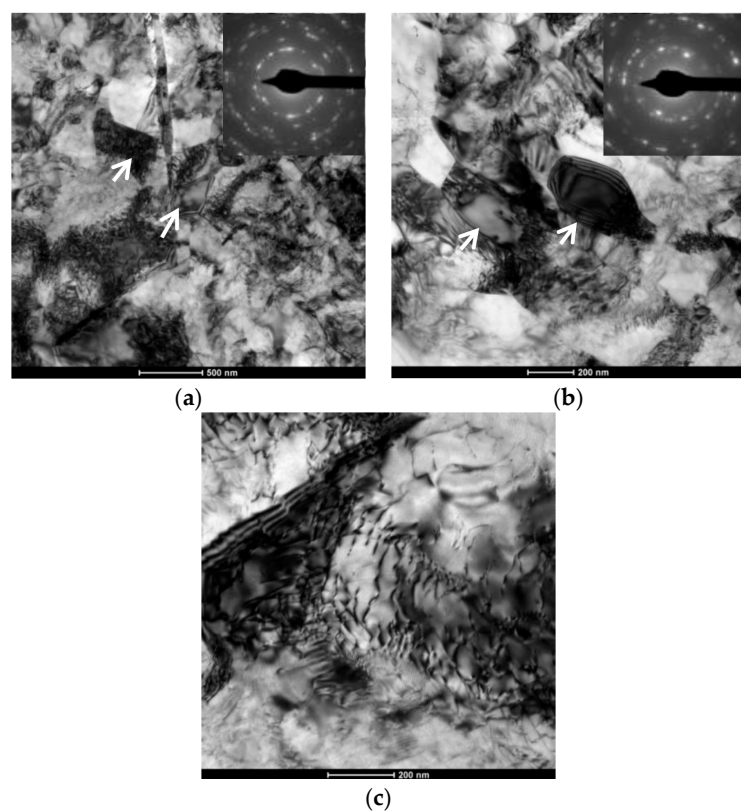


Figure 4. TEM (Transmission electron microscope) micrographs and corresponding SAED (Selected area electron diffraction) patterns of ECAP CP-Ti: (a) 4 passes; (b) 8 passes; (c) dislocations in 4 passes ECAP sample.

Continuous dynamic recrystallization (CDRX) could occur during high temperature deformation for metals with high stacking fault [16]. CDRX can promote the formation of sub-grains, and therefore refine the grain size. Many scholars had found that after eight passes ECAP, the grain size became larger than six passes or four passes ECAP sample [16,24]. Luo et al. [24] investigated the grain size evolution of CP-Ti during ECAP process with B_c route at 723 K, and found that the grain size was refined normally from two passes to four passes ECAP. However, when ECAP number was increased to eight passes, grains became coarse. The reason for this phenomenon could be attributed to the growing of DRX grains, as in their research CP-Ti had been subjected to repeated static annealing at the intervals of contiguous ECAP passes. In addition, Roodposhti et al. [16] approved the view that processing temperature could influence the refinement of grain size during the ECAP process. Higher temperature will promote the rate of recovery, and consequently dislocation annihilation becomes extensive which will lead to the decrease of dislocation density and increase of grain sizes [25,26].

In the case of this study, it is clear that with increasing the number of RD-ECAP passes, the grain size decreases continuously. The average grain size is about 500 nm after four passes RD-ECAP, which is almost 160 times finer than the original sample (80 μm). In addition, after the latter four passes ECAP, the grain size of eight pass ECAP (310 nm) is less than twice smaller compared with four-pass sample. However, it should be noted that the decrease in grain size after the latter four passes RD-ECAP is less obvious than initial four passes. This is because the refinement effect of ECAP is limited when initial microstructure is in sub-micron scale [27]. Previous study [28] showed that small grains may exhibit a low stability when metals are heavily deformed, and additional straining may occur as ECAP does not further reduce the grain size because of the intrinsic instability of nano-sized (below 100 nm) and submicrometre-sized (between 100 and 1000 nm) grains. There has been a dynamic balance of grain refinement between structure refinement and recovery (and coarsening) at ambient temperature [27]. Therefore, the grain refinement effect of ECAP exhibits a limit, and with a further increase of processing numbers, the grain size and dislocation density will achieve ultimate values. In order to further decrease the grain size, cold rolling (CR) was employed on ECAP CP-Ti in this work. CR is one of the most convenient ways to further process ECAP titanium, and recovery can hardly take place during rolling at room temperature [14,29].

3.2. Microstructure of ECAP + CR (Cold Rolling) CP-Ti

Figure 5 shows the optical microstructures of as-received and ECAP CP-Ti after cold rolling, and an obvious refining effect is observed after CR. It can be seen that CR process introduces a more homogeneous microstructure than the ECAP process, and grain size is refined obviously. Figure 6a shows the TEM micrograph of as-received CP-Ti after only CR process; it can be seen that the grain size is refined to about 3 μm , and some twins can be observed. However, it is hard to distinguish whether these twins were newly formed during CR or remained from the original microstructure. Figure 6b shows the TEM image of 4p-ECAP + CR sample; it is apparent that the grain size was further refined to 120 nm. In addition, high-density dislocations can be observed within finer grains, and the corresponding diffraction ring is more intensive and fluent than that of the ECAP sample, suggesting that there are more high-angle boundaries in ECAP + CR sample than four passes ECAP sample. As for 8p-ECAP + CR sample, it can be seen from Figure 6c that the grain size is decreased to 90 nm, almost forming a nano-grained (NG) CP-Ti. However, compared with 4p-ECAP + CR sample, the density of dislocations decreases.

During the CR process, accumulative strain continuously increases, as well as dislocations. As long as a dislocation cell is newly formed, it can absorb the high density dislocations inside the firstborn dislocation cell, and then transfer to the cell wall, thus a whole dislocation cell comes into being [16]. When these dislocation cells turn into high angle boundaries, the microstructure could be further refined. Based on the above considerations, it can be concluded that with the combination of multi-pass RD-ECAP and CR, a homogeneous UFG CP-Ti (even NG for 8p-ECAP + CR sample) is

obtained, suggesting that the combined ECAP + CR technique is an effective method for preparation of UFG/NG CP-Ti.

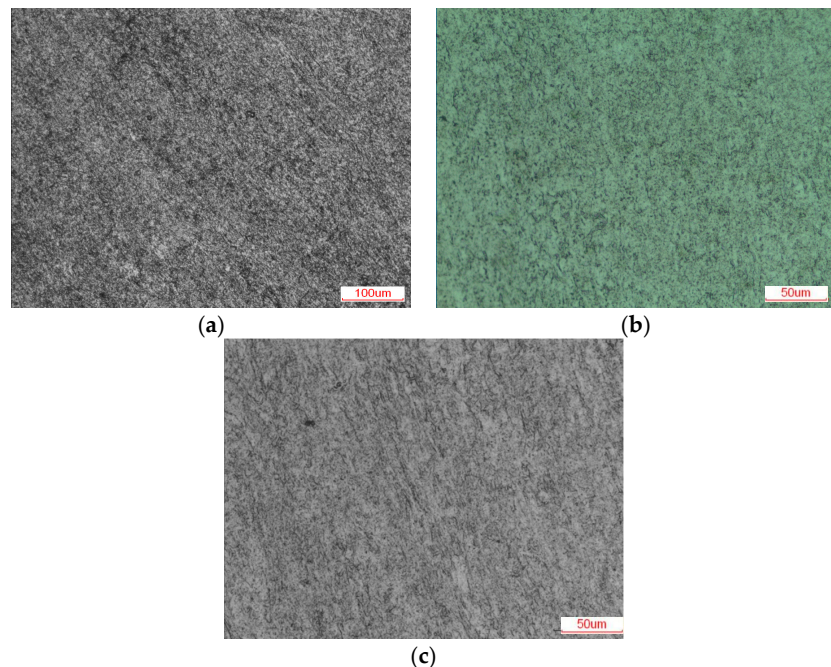


Figure 5. Optical micrographs of cold rolled CP-Ti: (a) AS (As-received) + CR; (b) 4p-ECAP + CR; (c) 8p-ECAP + CR.

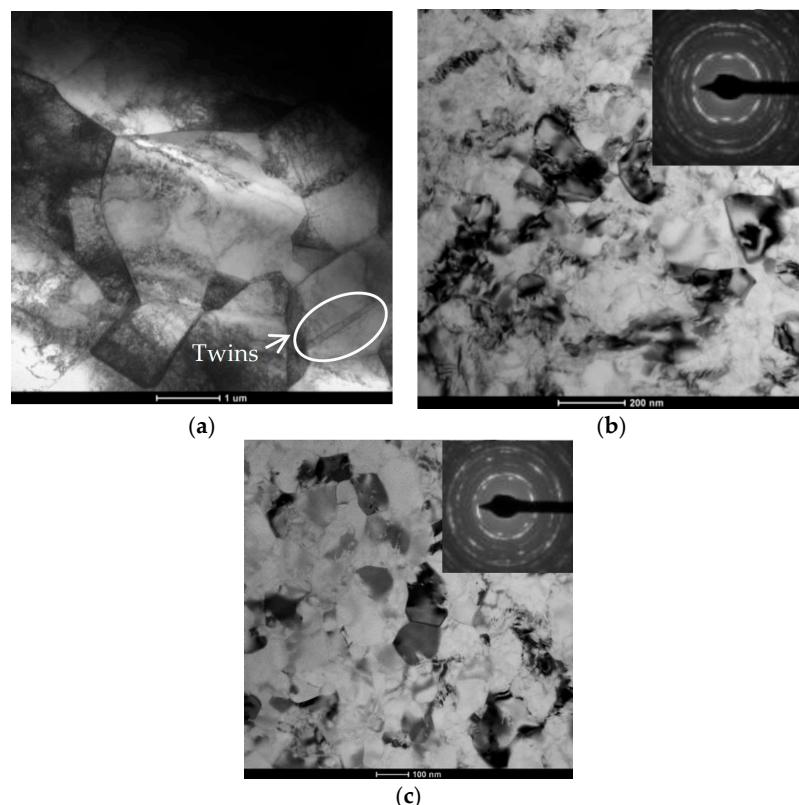


Figure 6. TEM micrographs and corresponding SAED patterns of cold rolled samples: (a) AS (As-received) + CR; (b) 4p-ECAP + CR; (c) 8p-ECAP + CR.

3.3. Mechanical Properties of CP-Ti at Different Processing Stages

Figure 7a shows the room temperature tensile curves of CP-Ti at different processing stages. Moreover, the variations of ultimate tensile strength (UTS), tensile yield strength (TYS), and strain to failure with different processing stages are also summarized in Figure 7b. The as-received sample exhibits a low UTS of 427 MPa and a high strain to failure of 45.3%. After four passes of ECAP, there is a boost of strength, which increased to 681 MPa, but the fracture strain decreased to 33.1%. As for 8p-ECAP sample, its UTS and fracture strain have decreased by 9% and 16%, respectively, when compared with that of 4p-ECAP sample. When as-received and ECAP CP-Ti were cold rolled, their strengths are improved remarkably, but their fracture strains are reduced. The as-received + CR sample shows high UTS of 799 MPa, which is almost twice that of the as-received sample, and is even higher than both ECAP samples, suggesting that cold rolling exhibits a more obvious strengthening effect than ECAP. However, its ductility is greatly decreased compared with ECAP metals. When ECAP metals are cold rolled, a more obvious improvement of strength is observed. The 4p-ECAP + CR and 8p-ECAP + CR metals display high strength with UTS of 923 and 912 MPa, and moderate ductility with fracture strain of 18.2% and 21.3%, respectively. Therefore, it can be concluded that the strengthening effect of combined ECAP + CR method is more effective than single CR or ECAP pressing. In addition, an ultra-fine grained (nano-grained) CP-Ti with both high strength and good ductility is successfully fabricated via the combination of ECAP and cold rolling.

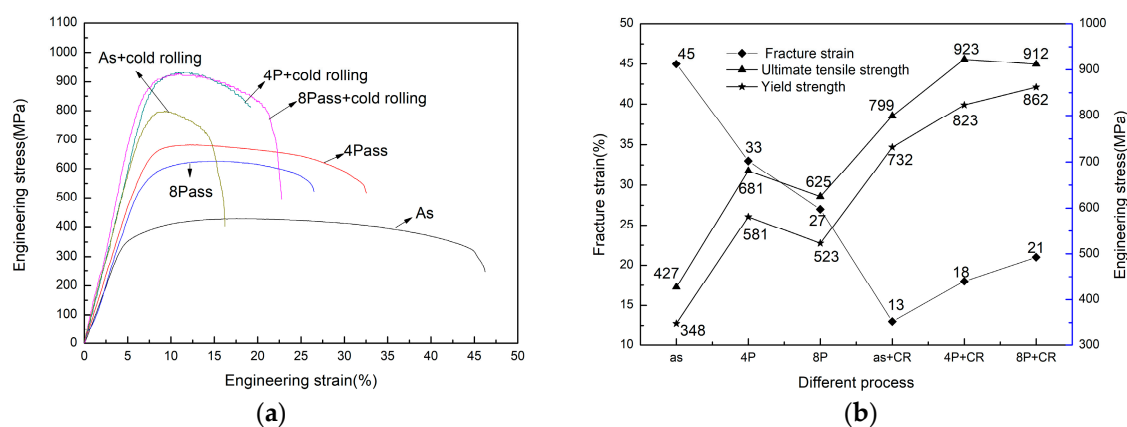


Figure 7. Mechanical properties of CP-Ti: (a) tensile curves of CP-Ti at different processing stages; (b) variation of ultimate tensile strength, tensile yield strength and fracture strain with different processing stages.

Moreover, Figure 8 shows the SEM micrographs of fracture appearance of CP-Ti after tensile tests. It is obvious that the dimples on the fracture surface of the as-received sample are bigger and deeper than other processed samples, which also demonstrates that the plasticity of the as-received sample is the best of all processing stages. As for ECAP metals, unequal-sized ovoid cavity appear, suggesting the existence of ductile fracture [30]. Seen from Figure 8d–f, the fracture surfaces of cold rolled samples exhibit more uniform characterizations with dense and shallow dimples. The decrease in dimple depth often implies the deterioration of ductility, which corresponds to the lower strain to failure in Figure 7.

Different technologies have already been employed to process high strength CP-Ti [4]. Figure 9 shows the comparison of mechanical properties of CP-Ti (grade 2) in this work and that fabricated via other different technologies in reference [8,11,27,29,31,32]. Stolyarov et al. [27,29] combined ECAP with CR and cold extrusion (CE) and successfully fabricated two high strength CP-Ti with high UTS of 1050 MPa. However, their elongations decreased obviously, which were 6% and 8%, respectively. Moreover, Stolyarov et al. [11] also employed two SPD methods together on processing of CP-Ti, and by this ECAP + HPT (high pressure torsion) method, CP-Ti gained a better elongation of 25% but with a lower strength of 730 MPa. It can be seen that in these studies, high strength and

high ductility were not attained simultaneously for CP-Ti. In addition, other SPD methods were also employed for processing of CP-Ti. Fattah-Alhosseini et al. [32] used accumulative roll bonded to process CP-Ti and a UTS of 989 MPa and elongation of 10% were obtained. Kim et al. [8] introduced high-radio differential speed rolling (HRDSR) on CP-Ti processing, and prepared CP-Ti with UTS of 895 MPa and elongation of 11%. Although the ductility was improved in these works, it still needs further improvement. In this work, when the RD-ECAP + CR combined method was carried out, although the ultimate tensile strength is a bit lower than some work, both high strength (above 900 MPa) and good ductility (above 20%) is attained for CP-Ti. This exhibits a better comprehensive mechanical property than previous works and the typical annealed Ti-6Al-4V (TC4) alloys (with UTS of 950 MPa and elongation of 14%) [33].

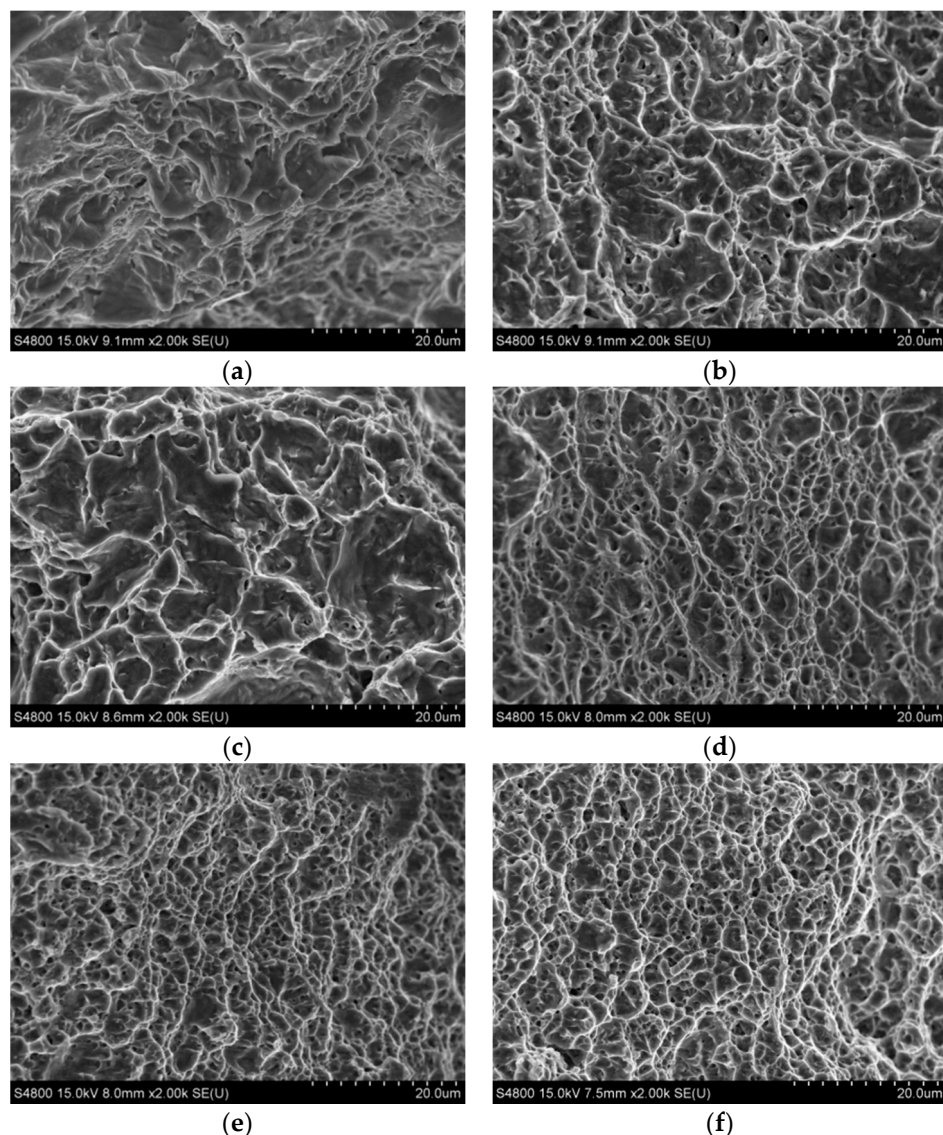


Figure 8. SEM micrographs of the tensile fracture of CP-Ti: (a) as-received; (b) 4p-ECAP; (c) 8p-ECAP; (d) as-received + CR; (e) 4p-ECAP + CR; (f) 8p-ECAP + CR.

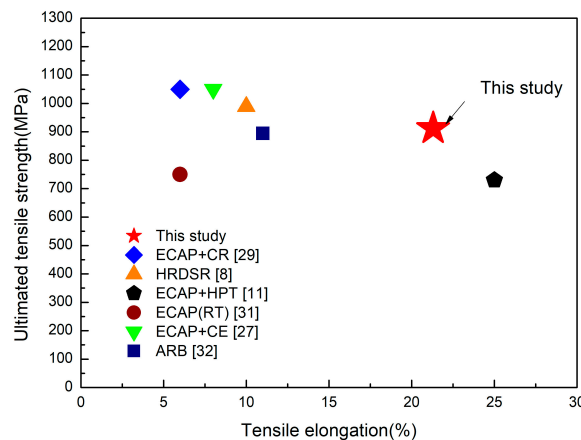


Figure 9. Comparison of mechanical properties of CP-Ti processed by different technologies in references [8,11,27,29,31,32] and in this work (HRDSR: high-radio differential speed rolling; HPT: high pressure torsion; RT: room temperature; CE: cold extrusion; ARB: accumulative roll-bonding).

3.4. Correlation between Microstructures and Mechanical Properties of CP-Ti

Grain size plays an important role in improving the strength of polycrystalline metallic materials [3,34]. Figure 10 shows the comparison of calculated Hall-Petch relationship for CP-Ti and the data obtained in this work. The Hall-Petch relationship is given by:

$$\sigma_{0.2} = \sigma_0 + Kd^{-1/2} \quad (1)$$

where $\sigma_{0.2}$ is the yield stress, σ_0 is a materials constant for the starting stress for dislocation movement (or the resistance of the lattice to dislocation motion), K is the strengthening coefficient (a constant specific to each material), and d is the average grain diameter. The coefficients σ_0 and K can be referred to reference [35] as $\sigma_0 = 182$ MPa and $K = 0.36$ MPa·m^{1/2}. It is generally accepted that Hall-Petch relationship is valid in submicrometer grains. When the grain size refined to around 100 nm, it has inverse Hall-Petch relationship, which has been reported by Tang et al. [36]. As for this work, it can be seen from Figure 10 that the strength of CP-Ti generally follows the well-known Hall-Petch relationship, even when the grain size has been refined to about 120 nm and 90 nm. However, it should be noted from Figure 10 that although the grain size for 8p-ECAP is finer than 4p-ECAP, the yield strength of 8p-ECAP is a little lower than 4p-ECAP. The same phenomenon is also observed for cold rolled ECAP samples. These abnormal phenomena imply that grain-boundary strengthening is not the only strengthening mechanism for CP-Ti obtained in this work.

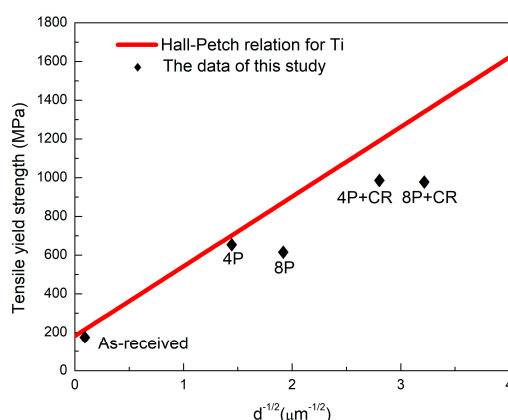


Figure 10. The Hall-Petch relation for Ti and the data of this study.

Combining the TEM micrographs and corresponding SAED patterns in Figures 4 and 6, it can be seen that the density of dislocations in 4p-ECAP sample is a little higher than 8p-ECAP, and it is the same situation in ECAP + CR samples. Therefore, the high-density dislocations may also play an important role in the strengthening of UFG CP-Ti.

To quantitatively analyze the evolution of dislocation densities with different processing stages, we evaluated the dislocation density by XRD according to the Williamson-Hall method [37,38]. Figure 11 shows the full width at half maximum (FWHM) of three representative peaks from XRD patterns of CP-Ti with different processing stages. It can be seen that after cold rolling, the FWHM exhibits a remarkable increase compared with that of ECAP CP-Ti. Previous studies [28] demonstrated that the increase of peak width is associated with grain refinement and higher dislocation density. Based on the Williamson-Hall method [39,40], the following formula can be deduced:

$$(\Delta K)^2 \cong \left(\frac{0.9}{D} \right)^2 + \left(\frac{\pi M^2 b^2}{2} \right) \rho K^2 \bar{C} + O(K^4 \bar{C}^2) \quad (2)$$

where $\Delta K = 2 \cos \theta (\Delta \theta) / \lambda$, $K = 2 \sin \theta / \lambda$, θ is the diffraction angle, λ is the X-ray wavelength, D is average particle size, ρ is the average dislocation density, b is the modulus of the Burgers vector of dislocations, \bar{C} is the average contrast factor of dislocations, and M is a constant depending on the effective outer cut-off radius of dislocation [39–41].

We have calculated the dislocation density from the above formula and the results are shown in Figure 12. It can be seen that the calculated dislocation density of 4p-ECAP alloy is a little higher than that of 8p-ECAP CP-Ti, which corresponds to TEM results. However, the dislocation density of ECAP CP-Ti is relatively low as the ECAP processing was conducted at a high temperature in this work. After cold rolling, the dislocation density increases remarkably regardless of the initial state before CR. Although 8p-ECAP + CR CP-Ti exhibits a little higher dislocation density than 4p-ECAP + CR CP-Ti, they are in the same magnitude order when considering the error limits. In addition, since the average grain size in 8p-ECAP + CR CP-Ti is smaller than 4p-ECAP + CR, and most dislocations are inclined to aggregate at grain boundaries, the dislocation density within α -Ti grains must be lower for 8p-ECAP + CR Ti than 4p-ECAP + CR Ti. The above obtained results are in good agreement with TEM observations in Figures 4 and 6, which further demonstrates that high-density dislocations contribute to strengthening of this UFG CP-Ti.

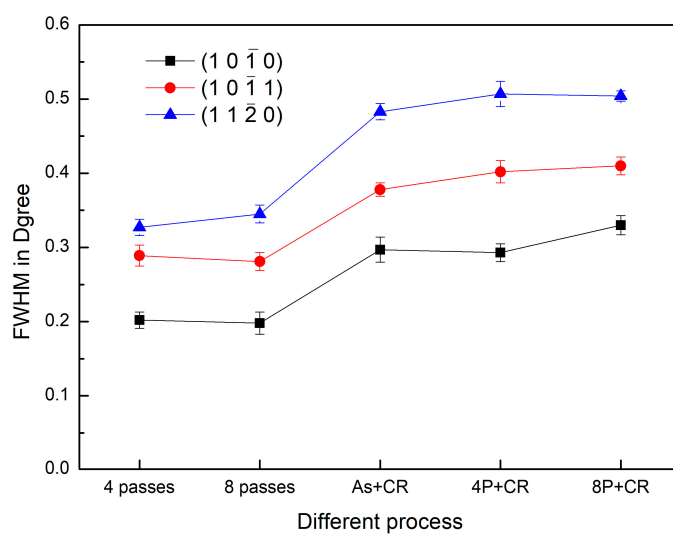


Figure 11. FWHM (full width at half maximum) for three characteristic peak of CP-Ti at different processing stage.

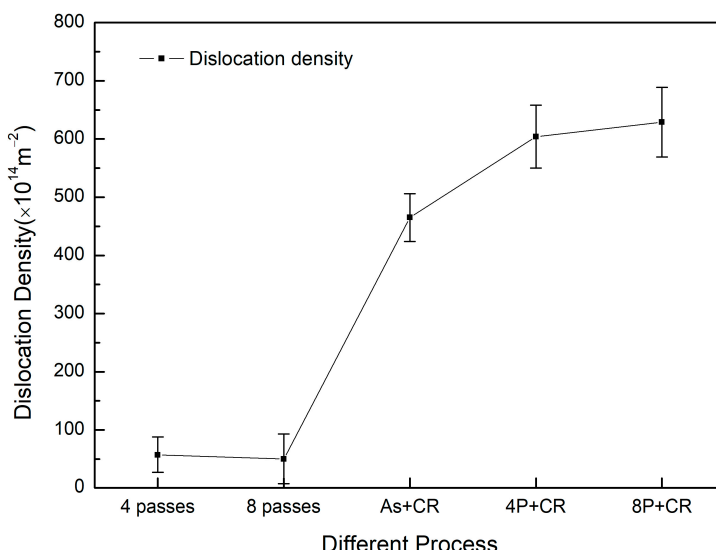


Figure 12. Evolutions of dislocation density in CP-Ti with different processing stages.

As for the good ductility of this UFG CP-Ti, it should be attributed to the increased fraction of high angle grain boundaries and the improved homogeneity of microstructures, which could increase the activation of grain boundary sliding and delay the propagation of cracks when they were nucleated during tensile [15,42].

Recently, it has been reported that $\alpha \rightarrow \omega$ and $\beta \rightarrow \omega$ phase transformations occurred for Ti-Fe alloys under high pressure deformation, and the mechanical properties might be improved after the high pressure phase transition [43,44]. Seen from Figure 9, two points are outside the strength-plasticity banana curve. One was prepared via combination of ECAP and HPT [11] and the other one is our work prepared via combined ECAP + CR. Both of these two studies are conducted under high pressure. However, during the XRD and TEM observations in our work and in reference [45], no phase transformation is confirmed, which might result from the relative lower Fe content in this CP-Ti, or from the undetectable metastable phase. In our further study, we will focus on phase transformations of CP-Ti or Ti-Fe alloys during the combined ECAP + CR processing.

Based on the above considerations, it can be concluded that the improved strength of UFG CP-Ti is attributed to the refined grain size and high density of dislocations, while the good ductility might result from the refined and more homogeneous microstructure after multi-pass RD-ECAP and CR.

4. Conclusions

In this work, the microstructure evolution and mechanical properties of CP-Ti (Grade 2) during multi-pass RD-ECAP and subsequent CR were systematically investigated, and a high-strength and good-toughness UFG CP-Ti was successfully fabricated. The main conclusions are summarized as follows:

- (1) The grain size of CP-Ti is effectively refined after the combination of RD-ECAP and CR. It decreases from 80 μm of as-received state to around 500 nm and 310 nm after 4 passes and 8 passes RD-ECAP, and further decreases to about 120 nm and 90 nm after subsequent CR processing.
- (2) XRD analysis shows that no phase transformation happens during ECAP + CR processing, and α -Ti is the only phase in these SPD CP-Ti. Moreover, calculated results by Williamson-Hall analysis of XRD and TEM observations demonstrate that the dislocation density increases remarkably after combination of ECAP and CR.
- (3) Room temperature tensile tests showed that CP-Ti after ECAP + CR exhibited the best combination of strength and ductility, with ultimate tensile strength and fracture strain reached 920 MPa and

20%, respectively. The high strength of this UFG CP-Ti originated mainly from refined grains and high density of dislocations, while the good ductility could be attributed to the increased activation of grain boundary sliding and improved homogeneity of UFG microstructure.

Acknowledgments: This work was supported by the National Natural Science Foundation of China (Grant No. 51774109), the Natural Science Foundation of Jiangsu Province of China (Grant Nos. BK20160869 and BK20160867), the Key Research and Development Project of Jiangsu Province of China (Grant No. BE2017148), the Fundamental Research Funds for the Central Universities (Grant No. HHU2016B10314), and the Postgraduate Research & Practice Innovation Program of Jiangsu Province (Grant Nos. 2017B779X14 and 2017B780X14).

Author Contributions: Haoran Wu, Jinghua Jiang and Aibin Ma conceived and designed the experiments; Haoran Wu, Ren Tang and Yanxia Gu performed the experiments; Haoran Wu, Xincan Zhao and Jiapeng Sun analyzed the data; Haoran Wu and Huan Liu wrote the paper. All authors have discussed the results, read and approved the final manuscript.

Conflicts of Interest: The authors declare no conflict of interest.

References

1. Leyens, C.; Peters, M. Titanium and titanium alloys: Fundamentals and applications. In *Titanium and Titanium Alloys*; John Wiley & Sons: Hoboken, NJ, USA, 2003; Volume 401, pp. 23–67.
2. Myers, J.R.; Bomberger, H.B.; Froes, F.H. Corrosion behavior and use of titanium and its alloys. *JOM* **1984**, *36*, 50–60. [[CrossRef](#)]
3. Sanosh, K.P.; Balakrishnan, A.; Francis, L.; Kim, T.N. Vickers and knoop micro-hardness behavior of coarse- and ultrafine-grained titanium. *J. Mater. Sci. Technol.* **2010**, *26*, 904–907. [[CrossRef](#)]
4. Valiev, R.Z.; Langdon, T.G. Principles of equal-channel angular pressing as a processing tool for grain refinement. *Prog. Mater. Sci.* **2006**, *51*, 881–981. [[CrossRef](#)]
5. Wang, C.T.; Gao, N.; Gee, M.G.; Wood, R.J.K.; Langdon, T.G. Effect of grain size on the micro-tribological behavior of pure titanium processed by high-pressure torsion. *Wear* **2012**, *280*–*281*, 28–35. [[CrossRef](#)]
6. Wang, X.J.; Xu, D.K.; Wu, R.Z.; Chen, X.B.; Peng, Q.M.; Jin, L.; Xin, Y.C.; Zhang, Z.Q.; Liu, Y.; Chen, X.H.; et al. What is going on in magnesium alloys? *J. Mater. Sci. Technol.* **2017**, in press. [[CrossRef](#)]
7. Liu, H.; Chen, Z.J.; Yan, K.; Yan, J.L.; Bai, J.; Jiang, J.H.; Ma, A.B. Effect of multi-pass equal channel angular pressing on the microstructure and mechanical properties of a heterogeneous Mg₈₈Y₈Zn₄ alloy. *J. Mater. Sci. Technol.* **2016**, *32*, 1274–1281. [[CrossRef](#)]
8. Kim, H.S.; Yoo, S.J.; Jin, W.A.; Kim, D.H.; Kim, W.J. Ultrafine grained titanium sheets with high strength and high corrosion resistance. *Mater. Sci. Eng. A* **2011**, *528*, 8479–8485. [[CrossRef](#)]
9. Valiev, R.Z.; Korznikov, A.V.; Mulyukov, R.R. Structure and properties of ultrafine-grained materials produced by severe plastic deformation. *Mater. Sci. Eng. A* **1993**, *168*, 141–148. [[CrossRef](#)]
10. Valiev, R.Z.; Estrin, Y.; Horita, Z.; Langdon, T.G.; Zechetbauer, M.J.; Zhu, Y.T. Producing bulk ultrafine-grain materials by severe plastic deformation. *JOM* **2006**, *58*, 33–39. [[CrossRef](#)]
11. Stolyarov, V.V.; Zhu, Y.T.; Lowe, T.C.; Lslamgaliev, R.K.; Valiev, R.Z. A two step SPD processing of ultrafine-grained titanium. *Nanostruct. Mater.* **1999**, *11*, 947–954. [[CrossRef](#)]
12. Liu, H.; Ju, J.; Lu, F.M.; Yan, J.L.; Bai, J.; Jiang, J.H.; Ma, A.B. Dynamic precipitation behavior and mechanical property of an Mg₉₄Y₄Zn₂ alloy prepared by multi-pass successive equal channel angular pressing. *Mater. Sci. Eng. A* **2017**, *682*, 255–259. [[CrossRef](#)]
13. Terada, D.; Inoue, S.; Tsuji, N. Microstructure and mechanical properties of commercial purity titanium severely deformed by ARB process. *J. Mater. Sci.* **2007**, *42*, 1673–1681. [[CrossRef](#)]
14. Stolyarov, V.V.; Zhu, Y.T.; Alexandrov, I.V.; Lowe, T.C.; Valiev, R.Z. Grain refinement and properties of pure Ti processed by warm ECAP and cold rolling. *Mater. Sci. Eng. A* **2003**, *343*, 43–50. [[CrossRef](#)]
15. He, X.M.; Zhu, S.S.; Zhang, C.H. Analysis of the grain refinement mechanism for commercial pure titanium by ECAP and SMAT. *Adv. Mater. Res.* **2014**, *937*, 162–167. [[CrossRef](#)]
16. Roodposhti, P.S.; Farahbaksh, N.; Sarkar, A.; Murty, K.L. Microstructural approach to equal channel angular processing of commercially pure titanium—A review. *Trans. Nonferr. Met. Soc. China* **2015**, *25*, 1353–1366. [[CrossRef](#)]
17. Zhao, X.; Fu, W.; Yang, X.; Langdon, T.G. Microstructure and properties of pure titanium processed by equal-channel angular pressing at room temperature. *Scr. Mater.* **2008**, *59*, 542–545. [[CrossRef](#)]

18. Meredith, C.S.; Khan, A.S. The microstructural evolution and thermo-mechanical behavior of UFG Ti processed via equal channel angular pressing. *J. Mater. Process. Technol.* **2015**, *219*, 257–270. [[CrossRef](#)]
19. Zhao, X.; Yang, X.; Liu, X.; Wang, X.; Langdon, T.G. The processing of pure titanium through multiple passes of ECAP at room temperature. *Mater. Sci. Eng. A* **2010**, *527*, 6335–6339. [[CrossRef](#)]
20. Kim, I.; Kim, J.; Shin, D.H.; Lee, C.S.; Hwang, S.K. Effects of equal channel angular pressing temperature on deformation structures of pure ti. *Mater. Sci. Eng. A* **2003**, *342*, 302–310. [[CrossRef](#)]
21. Nishida, Y.; Arima, H.; Kim, J.C.; Ando, T. Rotary-die equal-channel angular pressing of an Al-7 mass% Si-0.35 mass% Mg alloy. *Scr. Mater.* **2001**, *45*, 261–266. [[CrossRef](#)]
22. Liu, H.; Ju, J.; Bai, J.; Sun, J.P.; Song, D.; Yan, J.L.; Jiang, J.H.; Ma, A.B. Preparation, microstructure evolutions, and mechanical property of an ultra-fine grained Mg-10Gd-4Y-1.5Zn-0.5Zr alloy. *Metals* **2017**, *7*, 398. [[CrossRef](#)]
23. Gu, Y.X.; Ma, A.B.; Jiang, J.H.; Yuan, Y.C.; Li, H.Y. Deformation structure and mechanical properties of pure titanium produced by rotary-die equal-channel angular pressing. *Metals* **2017**, *7*, 297. [[CrossRef](#)]
24. Luo, P.; McDonald, D.T.; Zhu, S.M.; Palanisamy, S.; Dargusch, M.S.; Xia, K. Analysis of microstructure and strengthening in pure titanium recycled from machining chips by equal channel angular pressing using electron backscatter diffraction. *Mater. Sci. Eng. A* **2012**, *538*, 252–258. [[CrossRef](#)]
25. Yang, X.; Zhao, X.; Fu, W. Deformed microstructures and mechanical properties of CP-Ti processed by multi-pass ECAP at room temperature. *Rare Metall. Mater. Eng.* **2009**, *38*, 955–957.
26. Kim, I.; Kim, J.; Shin, D.H.; Park, K.T. Effects of grain size and pressing speed on the deformation mode of commercially pure Ti during equal channel angular pressing. *Metall. Mater. Trans. A* **2003**, *34*, 1555–1558. [[CrossRef](#)]
27. Stolyarov, V.V.; Zhu, Y.T.; Lowe, T.C.; Valiev, R.Z. Microstructure and properties of pure Ti processed by ECAP and cold extrusion. *Mater. Sci. Eng. A* **2001**, *303*, 82–89. [[CrossRef](#)]
28. Lu, K. Stabilizing nanostructures in metals using grain and twin boundary architectures. *Nat. Rev. Mater.* **2016**, *1*, 16019. [[CrossRef](#)]
29. Moradgholi, J.; Monshi, A.; Farmanesh, K. An investigation in to the mechanical properties of CP Ti/TiO₂ nanocomposite manufactured by the accumulative roll bonding (ARB) process. *Ceram. Int.* **2017**, *43*, 201–207. [[CrossRef](#)]
30. Nie, D.; Lu, Z.; Zhang, K. Grain size effect of commercial pure titanium foils on mechanical properties, fracture behaviors and constitutive models. *J. Mater. Eng. Perform.* **2017**, *26*, 1283–1292.
31. Zhang, Y.; Figueiredo, R.B.; Alhajeri, S.N.; Wang, J.T.; Gao, N.; Langdon, T.G. Structure and mechanical properties of commercial purity titanium processed by ECAP at room temperature. *Mater. Sci. Eng. A* **2011**, *528*, 7708–7714. [[CrossRef](#)]
32. Fattah-Alhosseini, A.; Keshavarz, M.K.; Mazaheri, Y.; Ansari, A.R.; Karimi, M. Strengthening mechanisms of nano-grained commercial pure titanium processed by accumulative roll bonding. *Mater. Sci. Eng. A* **2017**, *693*, 164–169. [[CrossRef](#)]
33. Purcek, G.; Yapici, G.G.; Karaman, I.; Maier, H.J. Effect of commercial purity levels on the mechanical properties of ultrafine-grained titanium. *Mater. Sci. Eng. A* **2011**, *528*, 2303–2308. [[CrossRef](#)]
34. Zhao, Z.; Chen, J.; Guo, S.; Tan, H.; Lin, X.; Huang, W.D. Influence of α/β interface phase on the tensile properties of laser cladding deposited Ti-6Al-4V titanium alloy. *J. Mater. Sci. Technol.* **2017**, *33*, 675–681. [[CrossRef](#)]
35. Luo, P.; McDonald, D.T.; Xu, W.; Palanisamy, S.; Dargusch, M.S.; Xia, K. A modified Hall-Petch relationship in ultrafine-grained titanium recycled from chips by equal channel angular pressing. *Scr. Mater.* **2012**, *66*, 785–788. [[CrossRef](#)]
36. Tang, Y.; Bringa, E.M.; Meyers, M.A. Inverse Hall-Petch relationship in nanocrystalline tantalum. *Mater. Sci. Eng. A* **2013**, *580*, 414–426. [[CrossRef](#)]
37. Woo, W.; Balogh, L.; Ungár, T.; Choo, H.; Feng, Z. Grain structure and dislocation density measurements in a friction-stir welded aluminum alloy using X-ray peak profile analysis. *Mater. Sci. Eng. A* **2008**, *498*, 308–313. [[CrossRef](#)]
38. Ungar, T.; Borbely, A. The effect of dislocation contrast on X-ray line broadening: A new approach to line profile analysis. *Appl. Phys. Lett.* **1996**, *69*, 3173–3175. [[CrossRef](#)]
39. Williamson, G.K.; Hall, W.H. X-ray line broadening from field aluminium and wolfram. *Acta Metall.* **1953**, *1*, 22–31. [[CrossRef](#)]

40. Williamson, G.K.; Smallman, R.E., III. Dislocation densities in some annealed and cold worked metals from measurement on the X-ray debye-scherrer spectrum. *Philos. Mag.* **1956**, *1*, 34–46. [[CrossRef](#)]
41. Schafler, E.; Zehetbauer, M.; Ungàr, T. Measurement of screw and edge dislocation density by means of X-ray Bragg profile analysis. *Mater. Sci. Eng. A* **2001**, *319*, 220–223. [[CrossRef](#)]
42. Gunderov, D.V.; Polyakov, A.V.; Semenova, I.P.; Raab, G.I.; Churakova, A.A.; Gimaltdinova, E.I.; Sabirov, I.; Segurado, J.; Situdikov, V.D.; Alexandrov, I.V.; et al. Evolution of microstructure, macrotexture and mechanical properties of commercially pure Ti during ECAP-conform processing and drawing. *Mater. Sci. Eng. A* **2013**, *562*, 128–136. [[CrossRef](#)]
43. Kilmametov, A.R.; Ivanisenko, Y.; Mazilkin, A.A.; Straumal, B.B.; Gornakova, A.S.; Fabrichnaya, O.B.; Kriegel, M.J.; Rafaja, D.; Hahn, H. The $\alpha \rightarrow \omega$ and $\beta \rightarrow \omega$ phase transformations in Ti-Fe alloys under high-pressure torsion. *Acta Mater.* **2018**, *144*, 337–351. [[CrossRef](#)]
44. Kilmametov, A.; Ivanisenko, Y.; Straumal, B.; Mazilkin, A.A.; Gornakova, A.S.; Kriegel, M.J.; Fabrichnaya, O.B.; Rafaja, D.; Hahn, H. Transformations of α' martensite in Ti-Fe alloys under high pressure torsion. *Scr. Mater.* **2017**, *136*, 46–49. [[CrossRef](#)]
45. Kim, H.S.; Kim, W.J. Annealing effects on the corrosion resistance of ultrafine-grained pure titanium. *Corros. Sci.* **2014**, *89*, 331–337. [[CrossRef](#)]



© 2017 by the authors. Licensee MDPI, Basel, Switzerland. This article is an open access article distributed under the terms and conditions of the Creative Commons Attribution (CC BY) license (<http://creativecommons.org/licenses/by/4.0/>).